Optical feedback interferometry for microscale-flow sensing study: numerical simulation and experimental validation

Yu Zhao, Julien Perchoux, Lucie Campagnolo, Thierry Camps, Reza Atashkhooei, Véronique Bardinal

Research Article | Vol. 24, No. 21 | 17 Oct 2016 | OPTICS EXPRESS 23849

Optics EXPRESS

Optical feedback interferometry for microscale-flow sensing study: numerical simulation and experimental validation

YU ZHAO,[1] JULIEN PERCHOUX,[1,*] LUCIE CAMPAGNOLO,[1] THIERRY CAMPS,[1] REZA ATASHKHOOEI,[1,2] AND VÉRONIQUE BARDINAL[1]

[1]*LAAS-CNRS, Université de Toulouse, CNRS, INP, INSA, UPS, Toulouse, France*
[2]*Centre for Sensors, Instruments and Systems Development (CD6)-UPC BarcelonaTech, 10 Rambla St. Nebridi, Terrassa E-08222, Spain*
[*]*perchoux@laas.fr*

Abstract: Optical feedback interferometry (OFI) performance for microscale-flow sensing is studied theoretically and experimentally. A new numerical modeling approach for OFI flow meter spectrum reproduction is presented in this work to study the optical effect on the signal due to the micro-scale channel geometry. Two well-defined frequency peaks are found in the OFI spectrum, this phenomenon can be attributed to the reflection of the forward scattered light on the channel rear interface. The flow rate measurement shows good accuracy over a range of fluid velocities from 16.8 mm/s to 168 mm/s, thus providing a promising tool to study and to optimize the OFI microfluidic sensor system.

OCIS codes: (280.3340) Laser Doppler velocimetry; (250.7260) Vertical cavity surface emitting lasers; (280.3420) Laser sensors; (280.2490) Flow diagnostics.

References and links

1. G. M. Whitesides, "The origins and the future of microfluidics," Nature **442**(7101), 368–373 (2006).
2. J. G. Santiago, S. T. Wereley, C. D. Meinhart, D. J. Beebe, and R. J. Adrian, "A particle image velocimetry system for microfluidics," Exp. Fluids **25**(4), 316–319 (1998).
3. M. Baker and H. Wayland, "On-line volume flow rate and velocity profile measurement for blood in microvessels," Microvasc. Res. **7**(1), 131–143 (1974).
4. L. Büttner, J. Czarske, and H. Knuppertz, "Laser-Doppler velocity profile sensor with submicrometer spatial resolution that employs fiber optics and a diffractive lens," Appl. Opt. **44**(12), 2274–2280 (2005).
5. L. Campagnolo, M. Nikolić, J. Perchoux, Y. L. Lim, K. Bertling, K. Loubière, L. Prat, A. D. Rakić, and T. Bosch, "Flow profile measurement in microchannel using the optical feedback interferometry sensing technique," Microfluid. Nanofluidics **14**(1–2), 113–119 (2013).
6. U. Zabit, O. D. Bernal, T. Bosch, and F. Bony, "MEMS accelerometer embedded in a self-mixing displacement sensor for parasitic vibration compensation," Opt. Lett. **36**(5), 612–614 (2011).
7. J. Perchoux and T. Bosch, "Multimode VCSELs for self-mixing velocity measurements," in *Proceedings of IEEE Conference on sensors* (IEEE, 2007), pp. 419–422.
8. S. Donati, M. Norgia, and G. Giuliani, "Self-mixing differential vibrometer based on electronic channel subtraction," Appl. Opt. **45**(28), 7264–7268 (2006).
9. R. Lang and K. Kobayashi, "External optical feedback effects on semiconductor injection laser properties," IEEE J. Quantum Electron. **16**(3), 347–355 (1980).
10. Y. Mitsuhashi, J. Shimada, and S. Mitsutsuka, "Voltage change across the self-coupled semiconductor laser," IEEE J. Quantum Electron. **17**(7), 1216–1225 (1981).
11. J. R. Tucker, Y. L. Lim, K. Bertling, A. V. Zvyagin, and A. D. Rakić, "Fluid flow rate measurement using the change in laser junction voltage due to the self-mixing effect," in *Proceedings of IEEE Conference on Optoelectronic and Microelectronic Materials and Devices,* (IEEE, 2006), pp. 192–195.
12. M. H. Koelink, F. F. M. de Mul, A. L. Weijers, J. Greve, R. Graaff, A. C. M. Dassel, and J. G. Aarnoudse, "Fiber-coupled self-mixing diode-laser Doppler velocimeter: technical aspects and flow velocity profile disturbances in water and blood flows," Appl. Opt. **33**(24), 5628–5641 (1994).
13. E. Figueiras, A. Humeau-Heurtier, R. Campos, R. Oliveira, L. F. R. Ferreira, and F. F. M. de Mul, "Laser Doppler flowmeters prototypes: Monte Carlo simulations validation paired with measurements," in *Proceedings of Biomedical Engineering Systems and Technologies* (Springer Berlin Heidelberg 2012), pp. 135–149.
14. C. Zakian, M. Dickinson, and T. King, "Particle sizing and flow measurement using self-mixing interferometry with a laser diode," J. Opt. A: Pure Appl. Opt. **7**(6), S445–S452 (2005).

#268325 http://dx.doi.org/10.1364/OE.24.023849
Journal © 2016 Received 15 Jun 2016; revised 5 Sep 2016; accepted 8 Sep 2016; published 5 Oct 2016

Optics EXPRESS

15. S. K. Ozdemir, S. Shinohara, S. Takamiya, and H. Yoshida, "Noninvasive blood flow measurement using speckle signals from a self-mixing laser diode: in vitro and in vivo experiments," Opt. Eng. **39**(9), 2574–2580 (2000).
16. M. Nikolić, E. Hicks, Y. L. Lim, K. Bertling, and A. D. Rakić, "Self-mixing laser Doppler flow sensor: an optofluidic implementation," Appl. Opt. **52**(33), 8128–8133 (2013).
17. Y. L. Lim, R. Kliese, K. Bertling, K. Tanimizu, P. A. Jacobs, and A. D. Rakić, "Self-mixing flow sensor using a monolithic VCSEL array with parallel readout," Opt. Express **18**(11), 11720–11727 (2010).
18. M. Norgia, A. Pesatori, and L. Rovati, "Self-mixing laser Doppler: a model for extracorporeal blood flow measurement," in *Proceedings of IEEE Conference on Instrumentation and Measurement Technology* (IEEE, (2010), pp. 304–307.
19. F. F. M. de Mul, M. H. Koelink, M. L. Kok, P. J. Harmsma, J. Greve, R. Graaff, and J. G. Aarnoudse, "Laser Doppler velocimetry and Monte Carlo simulations on models for blood perfusion in tissue," Appl. Opt. **34**(28), 6595–6611 (1995).
20. L. Scalise, W. Steenbergen, and F. de Mul, "Self-mixing feedback in a laser diode for intra-arterial optical blood velocimetry," Appl. Opt. **40**(25), 4608–4615 (2001).
21. K. Ozdemir, I. Ohno, and S. Shinohara, "A comparative study for the assessment on blood flow measurement using self-mixing laser speckle interferometer," IEEE Trans. Instrum. Meas. **57**(2), 355–363 (2008).
22. R. Kliese, Y. L. Lim, T. Bosch, and A. D. Rakić, "GaN laser self-mixing velocimeter for measuring slow flows," Opt. Lett. **35**(6), 814–816 (2010).
23. M. Wang, M. Lu, H. Hao, and J. Zhou, "Statistics of the self-mixing speckle interference in a laser diode and its application to the measurement of flow velocity," Opt. Commun. **260**(1), 242–247 (2006).
24. C. Zakian, M. Dickinson, and T. King, "Particle sizing and flow measurement using self-mixing interferometry with a laser diode," J. Opt. A: Pure Appl. Opt. **7**(6), S445–S452 (2005).
25. M. Nikolić, Y. L. Lim, K. Bertling, T. Taimre, and A. D. Rakić, "Multiple signal classification for self-mixing flowmetry," Appl. Opt. **54**(9), 2193–2198 (2015).
26. W. M. Wang, W. J. O. Boyle, K. T. V. Grattan, and A. W. Palmer, "Self-mixing interference in a diode laser: experimental observations and theoretical analysis," Appl. Opt. **32**(9), 1551–1558 (1993).
27. L. Goldberg, H. F. Taylor, A. Dandridge, J. F. Weller, and R. O. Miles, "Spectral characteristics of semiconductor lasers with optical feedback," IEEE J. Quantum Electron. **18**(4), 555–564 (1982).
28. A. Quirantes, F. Arroyo, and J. Quirantes-Ros, "Multiple light scattering by spherical particle systems and its dependence on concentration: a T-matrix study," J. Colloid Interface Sci. **240**(1), 78–82 (2001).
29. H. Moench, M. Carpaij, P. Gerlach, S. Gronenborn, R. Gudde, J. Hellmig, J. Kolb, and A. van der Lee, "VCSEL-based sensors for distance and velocity," Proc. SPIE **9766**, 97660A (2016).
30. H.-E. Albrecht, M. Borys, N. Damaschke, and C. Tropea, *Laser Doppler and Phase Doppler Measurement Techniques* (Springer Verlag, 2003).
31. M. Spiga and G. L. Morino, "A symmetric solution for velocity profile in laminar flow through rectangular duct," Int. Commun. Heat Mass Transf. **21**(4), 469–475 (1994).

1. Introduction

With the development of micro-nanotechnology during the last two decades, a significant progress has been made in integrated microfluidic devices. Thanks to the miniaturization and integration of the chemical procedure this change of scale can provide many advantages such as high speed, reduction of reagent consumption, short reaction time and lowered cost. Therefore microfluidic systems are of great interest in bio-medical and chemical engineering domains, such as clinical diagnostics of pathologies, single-cell analysis, manipulation, drug development and chemical synthesis [1]. In microfluidic systems such as droplet-based systems where the droplets contain the reagents and analytes, the flowing velocity inside the channel determines the duration of reaction or characterization, therefore flowing velocity or volume flow rate measurement is fundamental for the micro-scale flow study. Regarding the small size of the microfluidic systems, compact flowmetry tools have recently carried out strong interest and effort. Nowadays various optical technologies have been proposed, such as Dual-Slit (DS) [2], Particle Image Velocimetry (PIV) [3] and Laser Doppler Velocimetry (LDV) [4]. OFI as a very simple interferometric sensing technology based on the optical feedback effect in lasers was recently proposed for flowmetry at the micro-scale [5]. This type of interferometer has been earlier proposed to measure displacement [6], velocity [7] and vibration [8]. A part of the emitted laser beam reflected or scattered by a distant target re-enters the laser cavity where it interacts with the initial laser free-running light. This interaction results in a variation of the laser emission performances amongst which the output power [9] or the junction voltage [10] are the most widely used for sensing applications. In

Optics EXPRESS

the case of translating targets, such as particles in a flow, the back-scattered light is subject to a frequency shift due to the Doppler Effect and the target velocity can be retrieved after proper spectral analysis of the amplified variations of the laser parameters. Thanks to this very simple sensing scheme that induces numerous advantages such as compactness, self-alignment, non-invasive measurement and high spatial resolution, the OFI based flowmeter sensor is a promising tool in bio-medical or micro-scale chemical engineering systems.

Various works have been reported on OFI sensors for flowmetry [11–25] deploying channels with sizes ranging from ten microns to several millimeters. However most of the existing related studies concern millimeter scale fluidic systems, while only few of them are treating micro scale configurations. OFI based microfluidic flowmeter sensor study remains indeed challenging because of the many practical problems, especially with systems where the typical scale is smaller than 100 μm. First, when the laser is pointing onto the micro channel, a large amount of particles with different velocities scatter the laser light back to the laser cavity and each of them contributes to OFI signal with its own Doppler frequency shift. Thus it results in a complex signal with a continuous frequency spectrum. Second, the scattered light power is very weak, only 10^{-7}~10^{-4} times of the initial emission power and OFI signal easily submerses in the noise. Third, due to the extremely small size and construction complexity, the influences on the OFI spectrum of the fluidic system (e.g., reflection or interference occurring in the channel structure) have to be taken into account, as the laser beam suffers from various perturbations during the incident and feedback propagation.

To overcome the challenges mentioned above, an accurate approach is required to model the optical behavior in a microfluidic system and to predict the spectra characteristics of OFI signal in micro-scale flows. To the author's knowledge, there are only few models proposed for OFI microfluidic measurement [18,19] without considering the micro channel geometry influence on the OFI spectra. In the current paper, we implement a Monte Carlo method-based model to analyze the laser induced scattering behavior of the micro particles in the micro channel and to evaluate how the channel construction and the other components affect the scattered light propagation. In this model, the entire system is simulated using a commercial ray tracing software. This modeling effort allow for the determination of the back-scattered power fraction that is re-injected into the laser cavity. Then, a modified laser rate equations model, which is based on the classical Lang and Kobayashi equations [9], calculates the laser power changes induced by the back-scattered light. To investigate the validity of our models and simulation methodology, a series of experimental validations are presented.

2. Theory

2.1 Laser diode OFI behavior of single target

To describe the laser diode behavior under optical feedback modulation, a three mirror cavity model is established [26]. As shown in Fig. 1(a), the OFI system consists of two cavities, one is the laser active cavity of length L_c, and the other is the external cavity of length L_{ext} induced by the target. The system is modeled as a single cavity of length L_c with an equivalent complex amplitude reflectivity r_{eq} shown in Fig. 1(b).

In the case of a translating target and considering that the target reflectivity is very small (i.e., $r_{ext} << r_2$), the equivalent reflectivity r_{eq} can be expressed as [27]:

$$r_{eq} = r_2[1 + \xi \exp(j\omega_D t + j\Phi_D)] \tag{1}$$

$$\xi = \frac{r_{ext}(1 - r_2^2)}{r_2} \tag{2}$$

Optics EXPRESS

$$\omega_D = 2\pi\nu\frac{-2V_A}{c+V_A} \tag{3}$$

$$\Phi_D = 2\pi\nu\left(1+\frac{c-V_A}{c+V_A}\right)\frac{\tau_d}{2} \tag{4}$$

where, ξ is the coupling coefficient, ω_D the angular frequency shift induced by the Doppler Effect, c the light velocity in vacuum, ν the laser free-running frequency, V_A the target velocity component in laser direction ($V_A = V\cdot\sin\theta$), j the imaginary unit. Φ_D is the additional phase term and $\tau_d = \frac{n\cdot L_{ext}}{c}$ is the external roundtrip delay time within the external cavity of refractive index n.

Considering $V_A << c$, then:

$$\omega_D = 2\pi\cdot f_D \approx 2\pi\frac{-2nV_A}{\lambda} \tag{5}$$

$$|f_D| = \frac{2nV_A}{\lambda} \tag{6}$$

f_D is the frequency shift due to the Doppler Effect. Thus neglecting the multiple roundtrips in the external cavity, considering the lasing condition and solving the laser rate equations, the output power under OFI modulation can be deduced as:

$$P_{OFI} = P_0[1+m\cos(\omega_D t+\Phi_D)] \tag{7}$$

where P_0 is the initial unperturbed laser output power, and m the modulation index:

$$m = 4\xi\frac{\tau_p}{\tau_l} \tag{8}$$

where τ_p is the photon lifetime within the laser cavity, $\tau_l = \frac{2\bar{n}_0 L_c}{c}$ is the roundtrip time in the laser cavity and $\bar{n}_0$ the effective group refractive index.

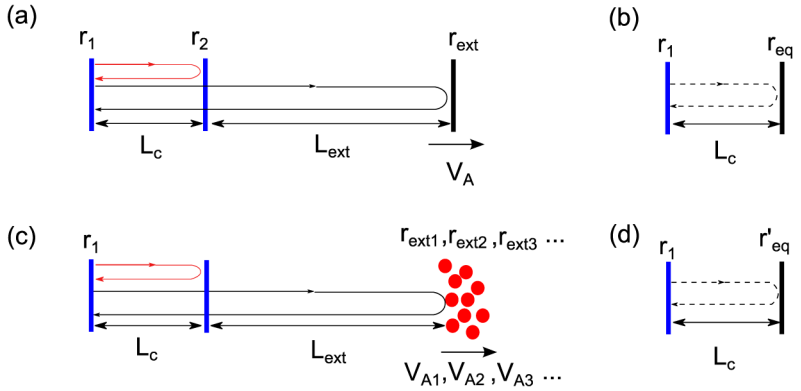

Fig. 1. Three mirror cavity model: (a) with a solid target, (c) with a group of small particles. Equivalent cavity: (b) with a solid target, (d) with a group of small particles.

2.2 OFI model with multiple scatterers

In the case of measurement in flows, the optical system collects the scattered light from a large amount of flowing particles (scatterers) of various velocities as indicated in Fig. 1(c)

Optics EXPRESS

and different positions in the measurement volume. This induces a distribution of the Doppler shifts that impact the LD output power spectrum.

In the case of a flowing solution where the particle concentration is low enough so that multiple interactions between incident photons and particles (multiple scattering) can be ignored, we can calculate the equivalent cavity reflectivity r_{eq}' by summing the back-scattering contributions from each particle yielding:

$$r_{eq}' = r_2[1+\sum_i \xi_i \exp(j\omega_{Di}t + j\Phi_{Di})] \tag{9}$$

$$\xi_i = \frac{r_{exti}(1-r_2^2)}{r_2} \tag{10}$$

$$\omega_{Di} = 2\pi\nu\frac{-2V_{Ai}}{c+V_{Ai}} \tag{11}$$

$$\Phi_{Di} = 2\pi\nu\left(1+\frac{c-V_{Ai}}{c+V_{Ai}}\right)\frac{\tau_{di}}{2} \tag{12}$$

$$\begin{aligned}\left|r_{eq}\right| &= r_2\sqrt{(1+\sum_i \xi_i\cos(\omega_{Di}t+\Phi_{Di}))^2+(\sum_i \xi_i\sin(\omega_{Di}t+\Phi_{Di}))^2} \\ &= r_2\sqrt{\begin{aligned}&1+2\sum_i \xi_i\cos(\omega_{Di}t+\Phi_{Di})+(\sum_i \xi_i\cos(\omega_{Di}t+\Phi_{Di}))^2 \\ &+(\sum_i \xi_i\sin(\omega_{Di}t+\Phi_{Di}))^2\end{aligned}}\end{aligned} \tag{13}$$

Considering $\xi_i << 1$, we can obtain:

$$\xi_i\cos(\omega_{Di}t+\Phi_{Di}) << 1 \tag{14}$$

$$\xi_i\sin(\omega_{Di}t+\Phi_{Di}) << 1 \tag{15}$$

So the third and fourth items in the square root can be neglected, and the absolute value of the equivalent reflectivity can be derived as:

$$\left|r_{eq}\right| = r_2\sqrt{1+2\sum_i \xi_i\cos(\omega_{Di}t+\Phi_{Di})} \tag{16}$$

The new modified P_{OFI}' from different scattering particles can be expressed:

$$P_{OFI}' = P_0[1+\sum_i m_i\cdot\cos(\omega_{D_i}\cdot t+\Phi_{D_i})] \tag{17}$$

From the Eq. (17), it can be concluded that in a fluidic system, the laser output power P_{OFI}' is determined by m_i and ω_{Di} which are related respectively to the reflection coefficient r_{exti} and the velocities component in laser direction V_{Ai} of the i^{th} particle. In the next section, both parameters are investigated through numerical simulation.

3. Material and methodology

3.1 Experimental setup

The schematic of the experimental setup designed for this study is shown in Fig. 2. The setup consists of a micro-scale channel (micro-reactor), the OFI based sensor with its optical arrangement, the data acquisition and the processing system.

Optics EXPRESS

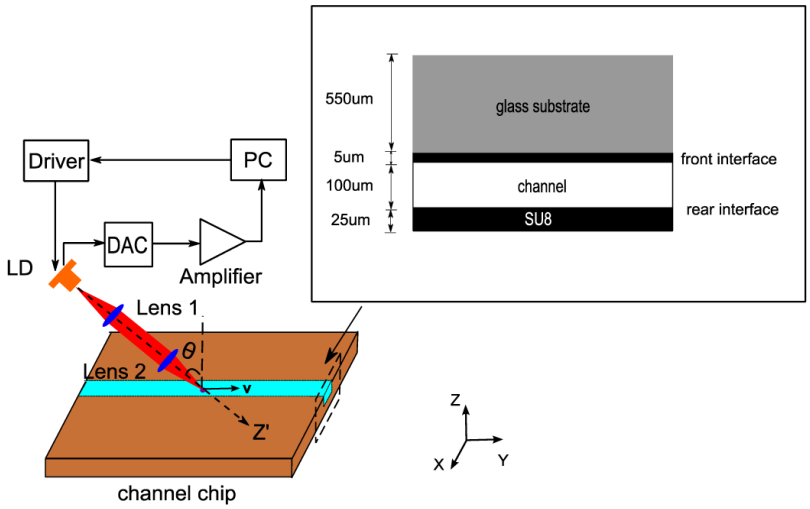

Fig. 2. Schematic of experiment setup (inset: cross-section view of the used microfluidic channel wafer).

The micro-reactor is a custom-designed square channel made of SU-8 photoresist with a 100 μm × 100 μm square cross-section. The schematic of the channel is presented in the inset of Fig. 2. Polystyrene (PS) micro spheres (MicroParticles, GmbH) are used as the scattering particles. PS micro spheres can be suspended very uniformly in aqueous solution after proper mixing due to their 1.05 g/cm^3 mass density which is similar to water. The PS solution with concentration 5 × 10^6 per mL is pumped into the channel by a syringe pressing pump (PHD 22/2000 Harvard Apparatus) in the Y direction as shown in Fig. 2. In such condition, the inter-particle distance is calculated to be about 58 μm (10 times of the particle diameter), so we can ensure the solution is in single scattering regime [28]. The flow rate is varied from 5uL/min to 50uL/min, i.e., velocities from 16.8 mm/s to 168 mm/s, respectively.

The OFI sensor is based on a commercial GaAs singlemode Vertical-Cavity Surface-Emitting Laser (VCSEL) in a TO-46 package that includes a monitoring photodiode (Optowell Co., Ltd). Such laser source presents the advantage of being compact and cost effective. Moreover the beam being of circular symmetry [29], it allows for an easier implementation in the modeling tools while providing with more generic results than with asymmetrical laser sources such as in-plane laser diodes. This laser source exhibits a good working performance at a wavelength of 670 nm with a 5° divergence angle (HWHM) and a circular beam with an intrinsic waist radius at 1/e^2 of 2.3 μm. It is operating under a constant bias current of 3.5 mA (1.5 times of the typical threshold current) using a custom designed laser driver. This bias value is chosen after weighting the tradeoff between the highest achievable signal-to-noise ratio while the laser remains operating in its singlemode regime. The incident angle θ between the laser emission axis Z′ and the perpendicular to the plane of the channel chip is set to 15°, as it is a good trade-off between maintaining a good signal-to-noise ratio and a sufficient Doppler shift frequency that fits our acquisition electronics.

Since the scattered light power is proportional to the power density, to enhance the feedback signal, high illumination power density is required. Tightly focused incident laser beam to minimize the laser spot area is a good way to increase the power density. Here we use a doublet lens pair (MAP103030B, Thorlabs Co., Ltd) constituted by two lenses that have the same focal length of 30 mm, so that the imaging magnification ratio is 1:1. Considering the VCSEL beam parameters, the focused 1/e^2 laser spot size in the micro-channel is calculated to be about 4.6 μm. The VCSEL and the lens pair are assembled on a 3D translation stage (T-LSR300A-KT03, Zaber Co., Ltd) which allows to adjust the beam focus position.

Optics EXPRESS

The OFI signal is acquired through the monitor photodiode embedded in the VCSEL package. The photodiode current is amplified using a custom made trans-impedance amplifier which output voltage is acquired using a National Instrument acquisition card (Ni USB 6251) at a sampling frequency of 400 kHz. Processing of the signal consist in 30 averagings of the Fast Fourier Transform (FFT) of 2^{14} samples length. All the data acquisition procedure and processing is automated by means of a dedicated LabVIEW VI.

3.2 Simulation methodology

The simulation of the OFI induced modulation of the laser diode emitted power in the microfluidic configuration requires several steps that are detailed below. First, a numerical modeling of the laser illumination into the micro channel is performed. Second, the particle induced scattering power towards the laser cavity is calculated. Both simulations are performed using the Monte Carlo method in a ray-tracing software (ZEMAX) and result in a calculated r_{exti} for each particle position in the channel. Third, a numerical simulation of the velocity distribution in the channel is conducted in computational fluid dynamics (CFD) software, Ansys Fluent, thus allowing for the determination of each V_{Ai}. Eventually, the rate equations model described above is computed using Matlab™ with the inputs established by the previous simulation steps and resulting in a time domain OFI signal from which a Fast Fourier Transform (FFT) is computed to obtain the OFI Doppler spectrum. All the simulation steps are described below.

3.2.1 Determination of the multiple particle reflectivity coefficient

Same as the realistic setup, in the ZEMAX simulation the laser beam propagates through the doublet lenses and several layers of different materials of the channel. Based on the manufacturer information, we define a 6 µm diameter circular surface (equal to the laser emitting aperture) placed on the front face of the VCSEL as the emission surface. Due to the specific configuration of the OFI, this area is also the feedback power detector area. The OFI configuration requires the use of the non-sequential tracing mode in which the rays are traced like in the actual physical order they hit various objects or surfaces, and where they can hit the same object repeatedly. For each position in the channel, one million rays are traced and amongst them, only the rare ones which are collected by the 6 µm diameter equivalent detector, after being scattered by the particles, are taken into account. In the simulation, all the object's parameters (e.g., geometrical sizes, materials, lens film coatings) are chosen to be a realistic reproduction of the experimental parameters presented previously (see Table 1).

As a very first step, to control the focal point position, the incident irradiant 2D profile through the channel is presented. Thus the channel position is set so that the focal point is at the channel center as illustrated in Fig. 3(a). A well-defined Gaussian irradiant profile in the channel center is obtained with a $1/e^2$ radius waist of 2.2 µm by Gaussian fitting, very close to the expected value (2.3 µm). Then a cuboid mesh (14 µm × 14 µm × 100 µm) is built in the channel for 3D mapping, the three dimensions grid intervals are set as: $dx = dy = 1$ µm, $dz = 0.5$ µm. For each coordinates, a 4.89 µm PS micro sphere is placed at the node position and the ray tracing is performed to calculate scattered light power fraction R_{ext}.

$$R_{exti} = \frac{P_{ini} - P_{ref}}{P_0} = \frac{P_{fdi}}{P_0} \tag{18}$$

$$r_{exti} = \sqrt{R_{exti}} \tag{19}$$

where P_0 is the unperturbed average emitted power, P_{ini} is the total power measured on the feedback detector, P_{ref} is the feedback power without the particle, and thus P_{fdi} is the feedback power contribution of the i^{th} particle.

Optics EXPRESS

Table 1. ZEMAX basic modeling parameters setting

Simulation parameters	Value
Wavelength	$\lambda = 670$ nm
Tracing ray number	$N = 10^6$
Emitting & detecting area diameter	$D_A = 6$ µm
Laser output $1/e^2$ radius	$w_0 = 2.3$ µm
Half divergence of laser beam	$\beta = 5$ °
Lens focal length	$f_1 = f_2 = 30$ mm
Refractive index of water	$n_{water} = 1.33$
Refractive index of SU8	$n_{su8} = 1.56$
Refractive index of glass substrate	$n_{glass} = 1.51$
PS particle diameter	$D_{ps} = 4.89$ µm
Refractive index of PS particles	$n_{ps} = 1.58$

The resulting 2D R_{ext} profile in the X-Z' plane is indicated in Fig. 3(b). The width of the 2D R_{ext} profile is approximately 14 µm, more than twice the one of the illumination volume profile. One reasonable explanation is that particles that are partially inside the illumination volume still induce a considerable scattered power contribution, so that the particle size impacts the R_{ext} profile.

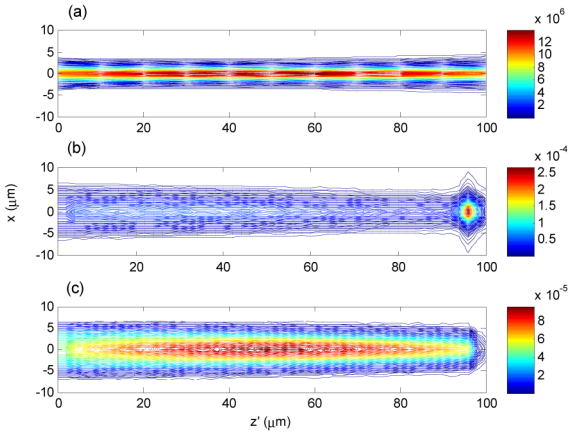

Fig. 3. 2D ZEMAX simulation mapping: (a) Incident irradiant 2D profile for laser focalization calibration; (b) Power fraction of back-scattered light profile in different particle positions with the rear interface and (c) in the case of an absorbing rear interface.

As can be observed in Fig. 3(b), the reflectivity distribution in the channel shows a maximum at a very short distance from the rear interface. This is the result of the forward scattered power that is in a second time back-scattered by the rear interface.

In Fig. 4, the simulated angular distribution of scattering intensity from a single particle is demonstrated, the scattered light intensity in the forward direction (0°) is more than 104 times higher than that the one in the backward direction (180°). Though the reflectivity of the rear interface is very low (less than 1% from Fresnel equations), there is still some forward scattered light reflected on the rear interface. When the particle is close enough from the rear interface, a significant portion of them will re-enter the LD cavity in the same way as the direct back-scattered light. This phenomenon is enhanced by the focusing behavior of the PS spheres that can be described using Debye series decomposition [30], and the "focal length" is related to the spherical particle diameter.

Optics EXPRESS

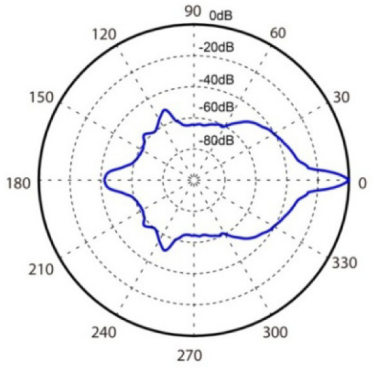

Fig. 4. Normalized scattered light irradiant profile simulated as a function of scatter angle.

To confirm the impact of the secondary back-scattered light, we have simulated the rear interface as a perfect absorbing medium. The direct back-scattered light from the micro sphere is the only light feedback source as can be observed in Fig. 3(c).

The simulated reflectivity distribution in this case and along the propagation axis is presented in Fig. 5 as well as the one of the actual SU8 rear interface. In the two hypotheses, a maximum reflectivity position is located at the channel center where the incident irradiance gets its maximal value. In the case of the SU8 rear interface (blue solid line) a very visible peak of reflectivity is observed with a maximum for particles center located at a distance of 5 µm from the rear interface. As expected it does not exist with the perfect absorbing rear interface (red dashed line).

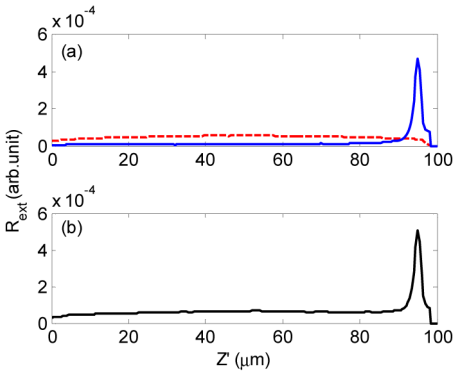

Fig. 5. Simulated profile of power reflectivity R_{ext} as a function of particle positions along laser emission direction (i.e., Z' direction). (a) The red dashed line and the blue solid curve correspond to the cases only considering the direct back-scattered light and the reflection of the forward scattered light on the rear interface, respectively. (b) The black curve describes the profile in the case of the realistic SU8 rear interface, where both R_{ext} contributions are taken into account.

3.2.2 Flow simulation

Flowing velocity distribution in the micro channel is conducted through a computational fluid dynamics (CFD) software ANSYS Fluent based on solving Navier-Stokes equations. Here we set the conditions in simulation as:the flow is laminar, the flowing liquid and the channel inner wall are incompressible and the inlet boundary condition is set as constant volume flow rate Q (in µL/min).

Optics EXPRESS

The velocity profile across the channel in the flow rate Q = 10 μL/min is depicted in Fig. 6. As expected, the maximum velocity is found at the channel center and the maximal velocity $V_{max}(Q)$ (in mm/s) is proportional to the flow rate Q [31]:

$$V_{\max}(Q) = 3.36 \times Q \tag{20}$$

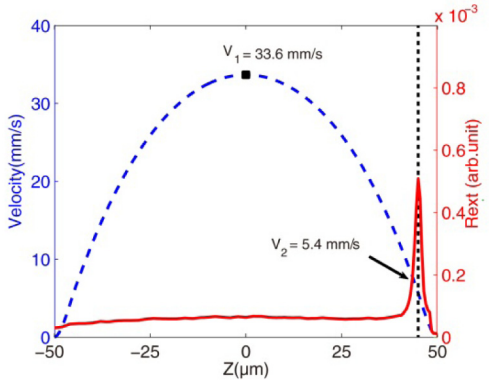

Fig. 6. Blue dashed curve depicts the Fluent-based velocity simulation profile along the laser axis (i.e., Z' direction) when the flow rate Q = 10 μL/min, with V_1 being the maximal value 33.6 mm/s in center. Red solid curve shows 1D power reflectivity coupling in laser direction. The sharp reflectivity peak demonstrates the region where the OFI signal is enhanced by the reflection of forward scattered light on the rear interface, and the black dot line shows the peak center position with a velocity V_2 of 5.4 mm/s.

3.2.3 Rate equation based OFI simulation

The modified power $P_{OFI}{}'$ in Eq. (17) is implemented with Matlab™ taking into account the r_{exti}, ω_{di} and τ_{di} calculated from previous simulation steps. The other parameters used are shown in Table 2. The OFI signals in all the particle positions are simulated separately, and then summed up. The time domain signal is transformed to the frequency domain via Matlab's FFT algorithm. The simulated spectra for different flow rates (20 μL/min and 40 μL/min) are plotted in Fig. 7. One of the most important results of this simulation is that there are two well-defined peaks in each spectrum. The low frequency (*fd1*) peak results from the forward scattered reflected light, and the frequency at the maximum of the peak corresponds to the Doppler shift induced by the velocity of the particles flowing at the R_{ext} peak position in Fig. 7. The second frequency peak (*fd2*) corresponds to the velocity at the other R_{ext} maximal position that is located at the center of the channel.

Table 2. Rate equations based OFI signal simulation parameters setting

Simulation parameters	Value
Photon lifetime in laser	$\tau_p = 10^{-12}$ s
Distance from laser to channel	L = 76 mm
Incidence angle	θ = 15 °
Laser output cavity mirror reflectivity	r_2 = 0.995

When increasing the flow rate parameter in the simulation, both spectral peaks shift towards higher frequencies while they tend to broaden because of larger velocity dispersion (see Fig. 7).

Optics EXPRESS

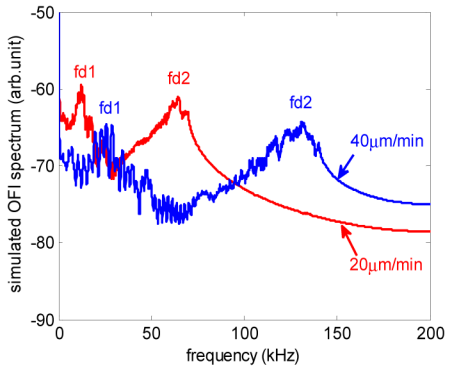

Fig. 7. Simulated OFI power spectra obtained for different flow rates (Q = 20 μL/min in red and 40 μL/min in blue).

4. Results and discussion

The OFI flow velocity measurements are performed with the setup depicted in section 3. In Fig. 8, the OFI signal spectrum simulated for a flow rate Q of 10μL/min (in red) compared with the measured one (in blue). As can be observed, the simulated and measured Doppler signals are quite resembling. In particular, both spectra have two visible frequency peaks: the lower frequency peak *fd1* corresponds to the reflection of the forward scattered light on the rear interface and the higher frequency *fd2* gives the velocity at the focus point, which is set in the channel center. Because of the original sharpness of the enhancement region as compared to the channel width as can be seen in Fig. 3(b), *fd1* is much sharper than *fd2*.

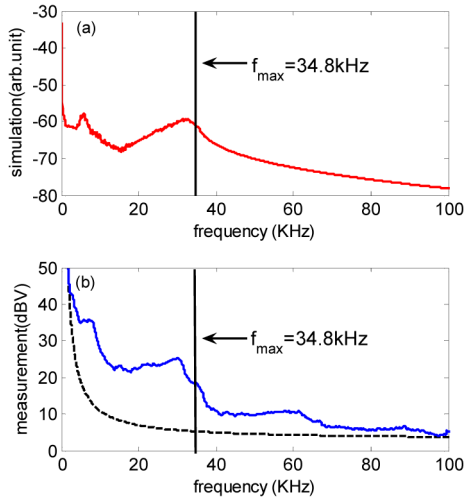

Fig. 8. Comparison of simulated OFI frequency spectrum red line in Fig. 8(a) and measured spectrum blue line in Fig. 8(b) when Q = 10μL/min. In both figures, there are two Doppler frequency peaks: *fd1* arises from the forward scattered light reflection on the rear interface and *fd2* denotes the velocity at the focus point. Two black solid lines indict the frequency (34.8 kHz) corresponding to the calculation based on maximal velocity (33.6 mm/s) from Fluent simulation. The black dashed line being calculated from the equation: $a / f + c$ for noise estimation, where a = 190, c = 4.

Another fact can be observed is that *fd1* in measurement is partly masked by the sensor low-frequency noise originating from either some remaining mechanical vibrations or the electronics Flicker noise. A *1/f* cure (black dashed line) is denoted for the noise level estimation in Fig. 8(b). These noise sources are not accounted in the simulation, so *fd1* in

Optics EXPRESS

simulation is still well-defined. On the other hand, in both cases *fd2* is a bit smaller than the frequency of the maximal velocity (f_{max} = 34.8 kHz) calculated from Eq. (6) and Eq. (20) (black solid line).

To validate the model efficiency, we have performed a study on the relationship between the flow rate *Q* and the Doppler frequencies extracted from measurement and simulations. We have kept the laser spot in the channel center and measured *fd1* and *fd2* for various values of *Q* ranging from 5 µL/min to 50 µL/min (equivalent to velocities from 16.8 mm/s to 168 mm/s according to the Fluent based model). This range corresponds to typical values encountered when monitoring blood flows in capillaries. For each flow rate, the measurements have been performed 3 times thus providing an estimation of the measurement repeatability and the robustness of the proposed numerical modeling method. However the robust determination of both *fd1* and *fd2* is not trivial. As can be seen in Fig. 9 where the OFI spectra measured at different flow rates (*Q* = 0 µL/min, 5 µL/min, 20 µL/min, 50 µL/min) the measured peak at *fd1* is not an integrated peak as in Fig. 8. Thus to extract central frequency in the first peak (*fd1*), a Gaussian curve-fitting has been employed. In the literature, *fd2* (the main Doppler frequency) is linked with the spectrum 3dB cutoff frequency [11,16] as depicted as well.

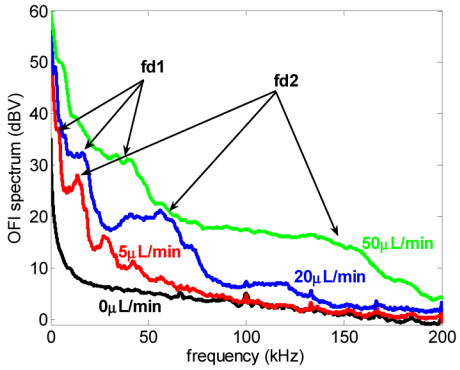

Fig. 9. Measured OFI spectral of various flow rates: *Q* = 0 µL/min (in black), *Q* = 5 µL/min (in red), *Q* = 20 µL/min (blue) and *Q* = 50µL/min (in green). Both *fd1* and *fd2* in each flow rate case are denoted as well.

Both data processing schemes mentioned previously for *fd1* and *fd2* are applied in the series of measurements and simulations under different flow rates. *fd1* trend as a function of *Q* is shown in Fig. 10: the values in simulation (black squares) and measurement (blue circles) are in good agreement over the whole given flow rate range, and both of them are consistent with the calculation frequency profile corresponding to the enhancement peak position in Fig. 6. This fact validates that *fd1* links to the particle velocity within this region where the OFI signal is enhanced by the forward scattered light reflection on the rear interface. It is noted that we performed similar measurements in PDMS channel of different depths, confirming the origin of this phenomenon. *fd2* versus *Q* profile is depicted in Fig. 11. Both fd1 and fd2 exhibit a linear dependence with the flow rate Q, as a result the ratio between the two frequencies remains constant (about 5 in our experimental conditions). While the simulation results are very close to the directly calculated value, the experiment results are slightly but consistently smaller than the simulation results. The position of the laser beam in the channel being controlled with accuracy not better than 10µm, a shift of the laser beam from the channel center is the most credible reason for this small discrepancy. Thus taking this hypothesis into account, and according to the Fluent simulation, the shift of the laser beam position can be estimated to 12 µm.

Optics EXPRESS

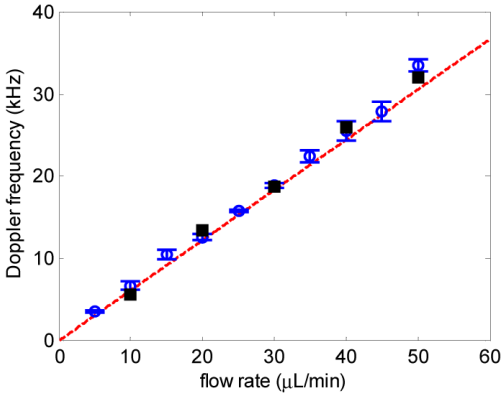

Fig. 10. Doppler frequency *fd1* trends as a function of the flow rate *Q*. The black solid markers correspond to the simulated values, and the blue hollow circles with error bars illustrate the measurement results. The red dashed line is the calculation result associated with the Fluent simulation velocity value in feedback power peak position in Fig. 6.

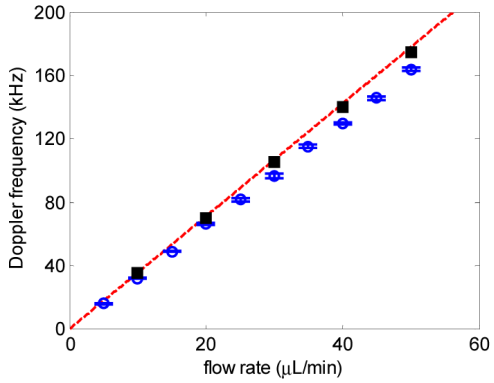

Fig. 11. Doppler frequency *fd2* profile versus different flow rates. The black solid markers and the blue hollow ones with error bars correspond to the simulated values and the measurement ones, respectively. The red dashed line is the calculation frequency curve associated with the maximal velocity values in channel center based on Eqs. (6) and (20).

5. Conclusion

In summary, we propose a novel modeling approach of the OFI sensing scheme in micro-scale fluidic systems. The OFI signal contribution of each scatterer is calculated by merging simulations results of the fluid flow, the optical system and the laser rate equations. This model has been validated by a series of experiments in an attractive and usable flow rate range (from 5 μL/min to 50 μL/min). With this model, one can predict the OFI sensor signal in any given microfluidic system even in the case of complicated reactors or flow regions. Furthermore, this method provides a promising tool to optimize the OFI flow sensor performances while designing micro-reactors with dedicated optical properties. We believe this modeling method is a first step to the design of future Lab-on-a-Chip devices requiring precise flow rate or fluid velocity monitoring.

The model presented in this paper for the first time predicts a second Doppler frequency peak that has been experimentally validated. This Doppler peak is proven to be due to the contribution to the optical feedback of flowing particles passing in the vicinity of the rear interface of the microreactor, and for which the forward scattering is reflected by this interface.

Optics EXPRESS

Funding

China Scholarship Council. People Programme (Marie Curie Actions) of the Seventh Framework Programme of the European Union (FP7/2007-2013) under REA grant agreement no. 600388 (TECNIO spring programme). LAA-CNRS micro and nanotechnologies platform member of the French RENATECH network. Business Competitiveness of the Government of Catalonia, ACCIÓ.

Acknowledgments

The authors gratefully acknowledge Véronique Conédéra and Rémi Courson for their contribution in microfluidic channel fabrication. The authors also sincerely appreciate Evelio R. Miquet's help in flow measurement work.